

ANDRZEJ JANKOWSKI
Polish Academy of Sciences
Institute of Oceanology — Sopot

EFFECT OF BOTTOM FRICTION ON THE STRUCTURE OF WIND-DRIVEN CIRCULATION

Contents: 1. Introduction, 2. Equations and boundary conditions, 3. Physical constants of the model, 4. The role of the bottom friction coefficient in the formation of circulation, 5. The field of surface currents, 6. The vertical structure of currents, 7. Conclusions; Streszczenie; References.

1. INTRODUCTION

This work is a continuation of a previous study by the author [3], in which the application of a hydrodynamical-numerical method (H-N) was analysed and necessary conditions were derived for the convergence of the short-wave approximation. The criteria derived depend on the bottom friction coefficient, space step of the numerical grid, and water depth. The two latter quantities are usually determined a priori (because of computer memory and size of water area), so that it is only the friction coefficient which can be chosen more arbitrarily.

This work deals with practical applications of the H-N scheme in the computations of the wind-driven circulation in an ideal water reservoir, by an analysis of the bottom friction coefficient in the formation of the circulation. The friction coefficient was considered in a number of versions, which were chosen to determine the effect of its magnitude and variability on the rate of approaching steady state of dynamic processes, the fields of mass transport, sea level, surface currents, and on the vertical distributions of current velocity components.

In the versions of the friction coefficient presented herein this parameter has been related to the vertical eddy viscosity. This made it possible to estimate the effect of both the friction and eddy viscosity on the circulation and correlate the two.

2. EQUATIONS AND BOUNDARY CONDITIONS

The system of differential equations for the computations of mass transport and sea levels takes the form [3]:

$$\frac{\partial M_x}{\partial t} - T_x + RM_x - \Omega M_y + \rho_0 g H \frac{\partial \xi}{\partial x} = 0 \quad (2.1)$$

$$\frac{\partial M_y}{\partial t} - T_y + RM_y + \Omega M_x + \rho_0 g H \frac{\partial \xi}{\partial y} = 0 \quad (2.2)$$

$$\frac{\partial \xi}{\partial t} + \frac{\partial M_x}{\partial x} + \frac{\partial M_y}{\partial y} = 0 \quad (2.3)$$

This system was found integrating the unsteady flow equations [1—3]:

$$\frac{\partial U}{\partial t} - A \frac{\partial^2 U}{\partial z^2} - \Omega V + g \frac{\partial \xi}{\partial x} = 0 \quad (2.4)$$

$$\frac{\partial V}{\partial t} - A \frac{\partial^2 V}{\partial z^2} + \Omega U + g \frac{\partial \xi}{\partial y} = 0 \quad (2.5)$$

$$\frac{\partial U}{\partial x} + \frac{\partial V}{\partial y} + \frac{\partial W}{\partial z} = 0 \quad (2.6)$$

carried out from the bottom to the sea surface. The boundary conditions were:

$$W = \frac{\partial \xi}{\partial t} + U_\xi \frac{\partial \xi}{\partial x} + V_\xi \frac{\partial \xi}{\partial y} \quad (2.7)$$

$$\rho_0 A \frac{\partial U}{\partial z} = T_x; \quad \rho_0 A \frac{\partial V}{\partial z} = T_y \quad (2.8)$$

at the surface $z = \xi$ and

$$W = -U_H \frac{\partial H}{\partial x} - V_H \frac{\partial H}{\partial y} \quad (2.9)$$

$$\rho_0 A \frac{\partial U}{\partial z} = RM_x; \quad \rho_0 A \frac{\partial V}{\partial z} = RM_y \quad (2.10)$$

at the bottom $z = -H$

in which:

U, V, W — components of current velocity along the axes x, y, z of the Cartesian system of coordinates, the origin of which is located on the free surface, the x -axis being oriented to the east — the y -axis to the north, and the z -axis vertically, upwards,

ξ — sea level,

R — bottom friction coefficient,

A — vertical eddy viscosity,

ρ_0 — water density (assumed constant),

Ω — Coriolis parameter,

H — water depth.

g — acceleration due to gravity,

T_x, T_y — tangential wind stress components,

$M_x = \int_{-H}^z \rho_0 U dz$ — x-component of mass transport,

$M_y = \int_{-H}^z \rho_0 V dz$ — y-component of mass transport.

The initial and boundary conditions of the system of equations (2.1—2.3) are as follows:

$$t = 0$$

$$M_x = M_y = \xi = 0$$

$$M_n|_L = 0$$

in which:

- L — shore line,

- M_n — mass transport component normal to shore line.

The finite-difference form of equations (2.1—2.3) in the H—N scheme [3] is:

$$\begin{aligned} M_{xm+1,n}^{t+\tau} &= M_{xm+1,n}^{t-\tau} (1 - 2R\tau) + 0,5 \Omega \tau \bar{M}_y - \\ &- \frac{g\tau}{h} H_{m+1,n} (\xi_{m+2,n}^t - \xi_{m,n}^t) + 2\tau T_{xm+1,n} \end{aligned} \quad (2.11)$$

$$\begin{aligned} M_{ym,n+1}^{t+\tau} &= M_{ym,n+1}^{t-\tau} (1 - 2R\tau) - 0,5 \Omega \tau \bar{M}_x - \\ &- \frac{g\tau}{h} H_{m,n+1} (\xi_{m,n+2}^t - \xi_{m,n}^t) + 2\tau T_{ym,n+1} \end{aligned} \quad (2.12)$$

$$\xi_{m,n}^{t+2\tau} = \xi_{m,n}^t - \frac{\tau}{h} (M_{xm+1,n}^{t+\tau} - M_{xm-1,n}^{t+\tau} + M_{ym,n+1}^{t+\tau} - M_{ym,n-1}^{t+\tau}) \quad (2.13)$$

in which:

$$\bar{M}_x = M_{xm+1,n+2}^{t-\tau} + M_{xm-1,n}^{t-\tau} + M_{xm+1,n}^{t-\tau} + M_{xm-1,n+2}^{t-\tau}$$

$$\bar{M}_y = M_{ym+2,n+1}^{t-\tau} + M_{ym,n+1}^{t-\tau} + M_{ym,n-1}^{t-\tau} + M_{ym+2,n-1}^{t-\tau}$$

τ, h — time and space steps of the numerical scheme,

m, n — indices of grid nodes along the x-axis and y-axis, respectively.

The stability criteria of the finite-difference scheme (2.11—2.13) in the short-wave approximation are [3]:

$$\tau \leq \frac{1}{R}; \quad \tau \leq \frac{1}{2R} \quad (2.14)$$

$$\tau \leq -\frac{Rh^2}{2gH} + \frac{h}{\sqrt{4gH}} \quad (2.15)$$

The current velocity components are computed from the relationship [3]:

$$\begin{aligned} D &= \frac{T}{\rho_0 Ak_1} \frac{ch k_1 (H+z)}{sh k_1 (H+\xi)} - \frac{RM}{\rho_0 Ak_1} \frac{ch k_1 (z-\xi)}{sh k_1 (H+\xi)} + \\ &+ \frac{g}{\Omega} i \left[\frac{\partial \xi}{\partial x} + i \frac{\partial \xi}{\partial y} \right] \end{aligned} \quad (2.16)$$

in which:

$$i = \sqrt{-1}; \quad D = U + iV; \quad T = T_x + iT_y$$

$$k_1 = \sqrt{i \frac{\Omega}{A}}; \quad M = M_x + iM_y$$

This relationship was found by integration of the steady-state equations (2.4 and 2.5) with the boundary conditions (2.8—2.10) assuming that the unknown values of mass transport and sea levels were computed numerically from equations (2.1—2.3).

In the derivation of relationship (2.16) it was also assumed that the vertical eddy viscosity A is independent of the vertical coordinate z.

3. PHYSICAL CONSTANTS OF THE MODEL

The parameters T_x , T_y , R, A in equations (2.1—2.3 and 2.16) should be determined prior to the computations.

The tangential wind components T_x , T_y are computed from the relationships [2, 4]:

$$T_x = \gamma W W_x \quad (3.1)$$

$$T_y = \gamma W W_y \quad (3.2)$$

in which:

W_x , W_y , W — wind velocity components and absolute value,
 $\gamma = 3.26 \cdot 10^{-6}$.

The bottom friction coefficient R and the vertical eddy viscosity A are computed from the following algorithms:

Version 1

The coefficient R is expressed by the Ekman formula [4]:

$$R = \frac{\pi A}{4H^2}$$

in which the eddy viscosity A should be found from the Felzenbaum theory [2] for a deep sea

$$A = 4.7 \cdot 10^{-8} \frac{W^2}{\Omega}.$$

Version 2

The coefficient R is computed as in version 1, while the eddy viscosity is determined by the Felzenbaum theory [2], for both a shallow sea and a deep sea:

$$A_1 = 0.54 \cdot 10^{-4} WH \quad H \leq H_{cr}$$

$$A_2 = 4.7 \cdot 10^{-8} \frac{W^2}{\Omega} \quad H > H_{cr}$$

jeżeli:

$$H_{cr} = 8.7 \cdot 10^{-4} \frac{W}{\Omega} = \text{critical depth dividing the shallow-water and deep-water areas.}$$

Version 3

The coefficients R and A are constant for the whole area and are chosen independently of each other.

Version 4

The coefficient R — constant as in version 3,
the coefficient A — computed as in version 1.

Version 5

The coefficient R — constant as in version 3,
the coefficient A — varies as in version 2.

4. THE ROLE OF THE BOTTOM FRICTION COEFFICIENT IN THE FORMATION OF CIRCULATION

In the computations it is assumed that a homogeneous rectangular water basin 260×160 km in size has a bottom profile as shown in Fig. 1, being constant along the y-axis. The circulation is driven by wind blowing along the y-axis at a speed of $W = 10 \text{ ms}^{-1}$ constant over the whole water area. The distribution of the network points in the water basin is shown in Fig. 2. The space step of the grid is $h = 10 \text{ km}$, while the Coriolis parameter is taken as $\Omega = 1.12 \cdot 10^{-4}$. The time step in our computations depends only on the bottom friction coefficient (2.14 and 2.15). The varia-

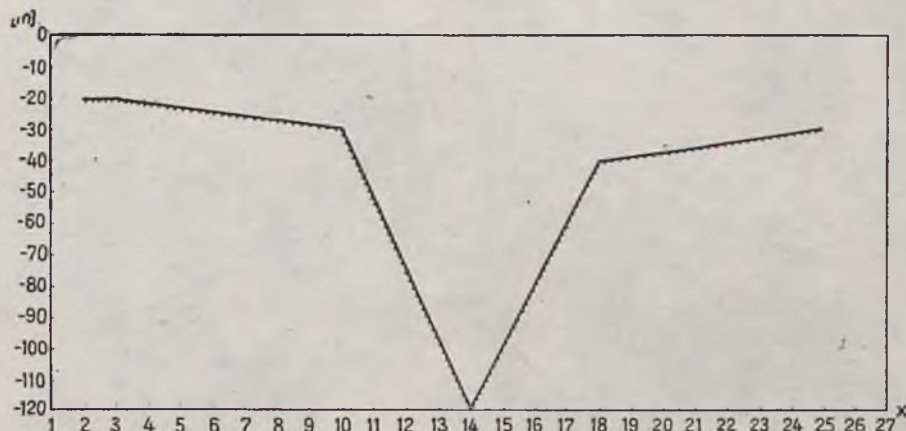


Fig. 1. Profile of bottom topography along x-axis

Ryc. 1. Profil dna akwenu wzduż osi OX

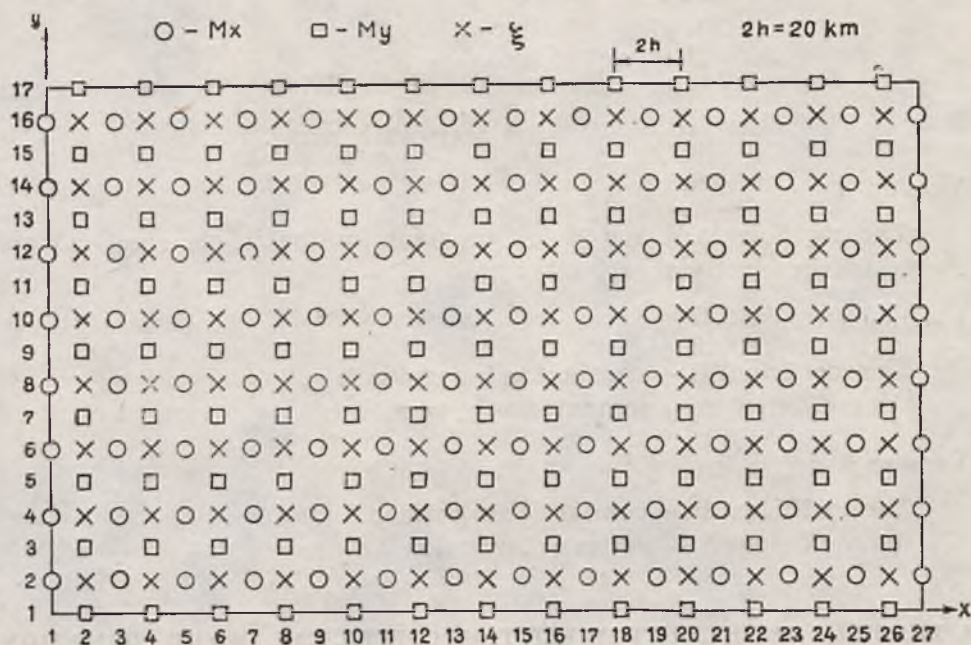


Fig. 2. Projection of numerical grid on OXY plane

Ryc. 2 Rzut siatki numerycznej na płaszczyznę OXY

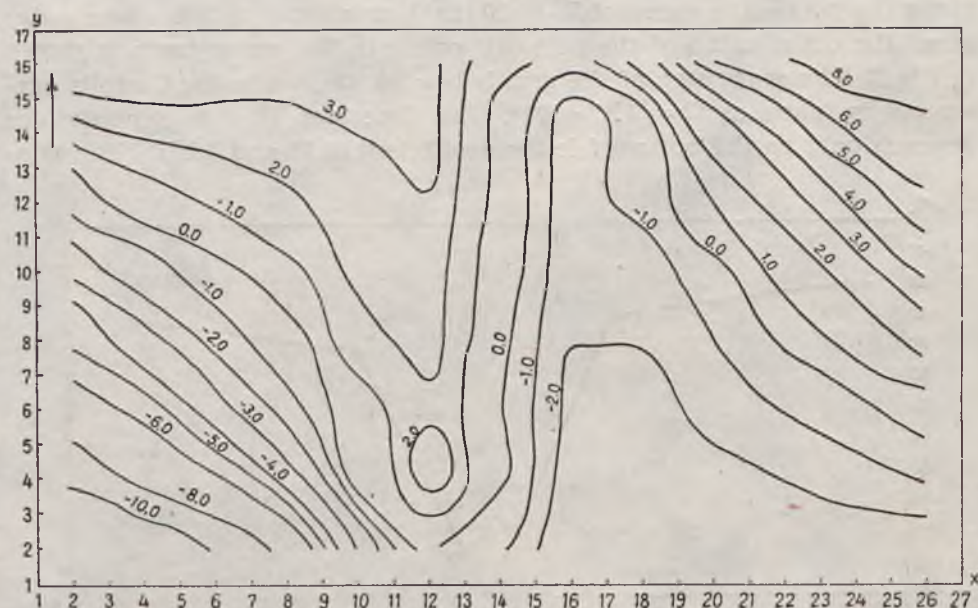


Fig. 3. Sea level distribution (cm) for case 1

Ryc. 3. Pole poziomu morza (cm) dla wariantu 1

bility of the parameter R throughout the different versions is illustrated in Table 1. Preliminary computations made it possible to determine that an adequate time step for the versions is $\tau = 1$ minute.

The development of the dynamic processes in time was analysed on the example of sea level. The computations carried out have shown that the water level surface assumes a steady form after 6910 time steps in version 1, after 14256 in version 2, and after 18 550 in versions 3, 4 and 5, for identical bottom friction in all versions and for the given accuracy of $\Delta\xi = 0.001$ cm — see Table 1.

The results of the computations are shown in Figs 3—8. From an analysis of the drawings it follows that the general picture of mass transport and sea level fields is similar in all versions, although there is a closer similarity in versions 2 and 3. The discrepancies between respective values of mass transport and sea levels are highest in the shallow-water zone, in which the values of the bottom friction coefficient in individual versions differ most.

5. THE FIELD OF SURFACE CURRENTS

The computations were run for five versions of the coefficients R and A (see Table 1). The results are presented in Figs. 9 to 13.

The general configuration of the current fields is similar in all cases, although the magnitudes of current velocity vectors at different points of the water area indicate considerable variability.

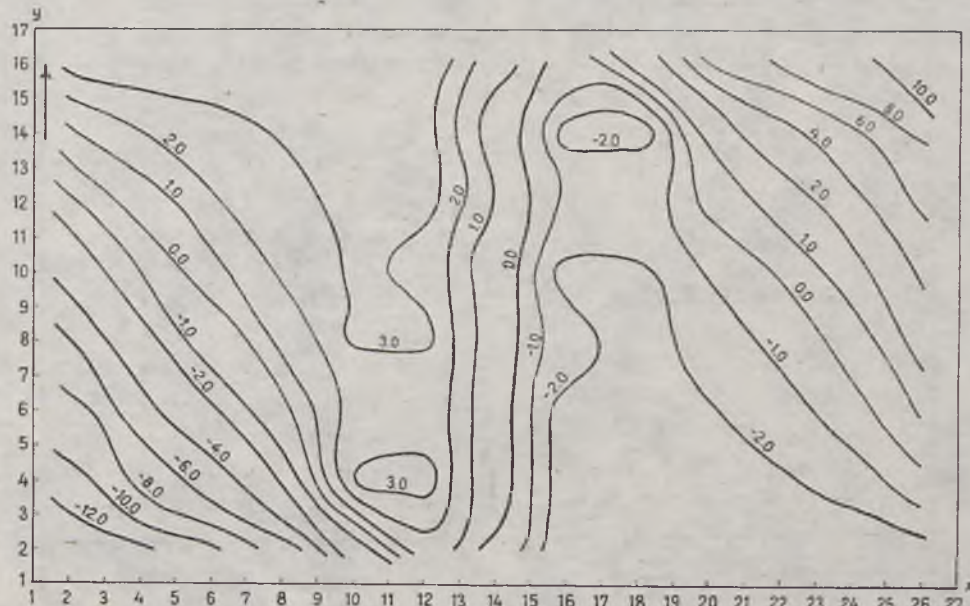


Fig. 4. Sea level distribution (cm) for case 2

Ryc. 4. Pole poziomu morza (cm) dla wariantu 2

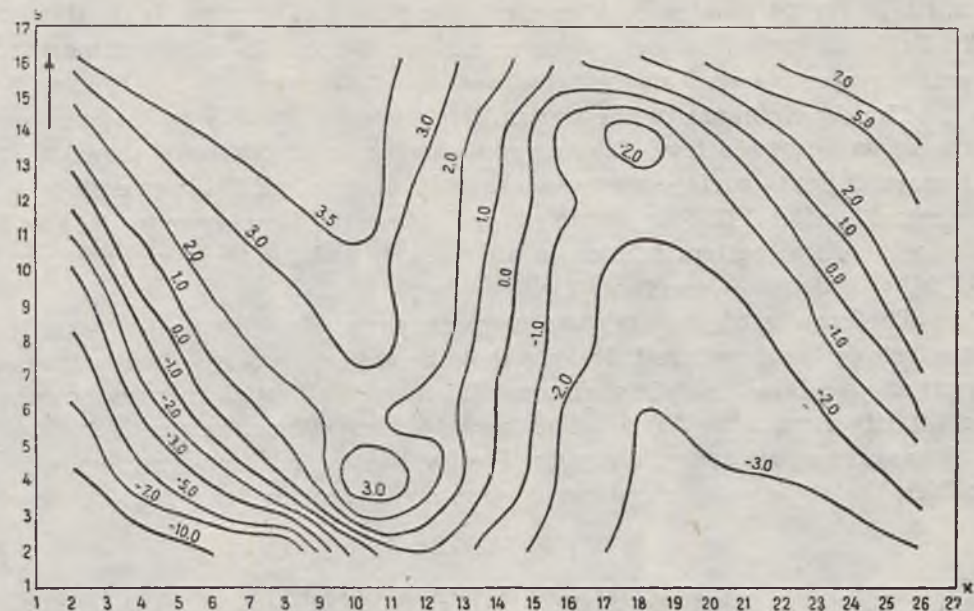


Fig. 5. Sea level distribution (cm) for case 3
Ryc. 5. Pole poziomu morza (cm) dla wariantu 3

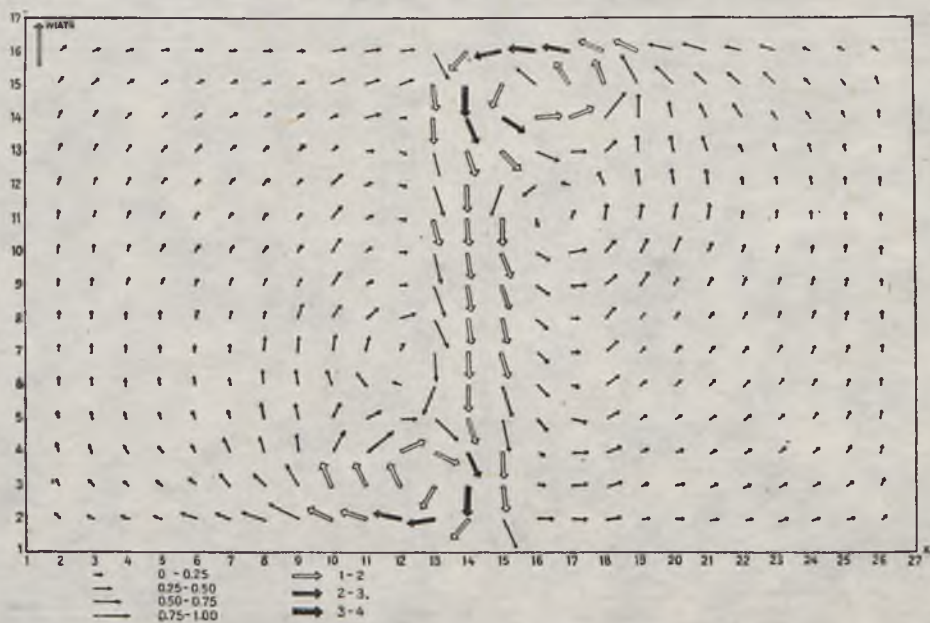


Fig. 6. Field of mass transport vectors ($10^5 \text{ g cm}^{-1} \text{ s}^{-1}$) for case 1
Ryc. 6. Pole wydatków masowych ($10^5 \text{ g cm}^{-1} \text{ sek}^{-1}$) dla wariantu 1

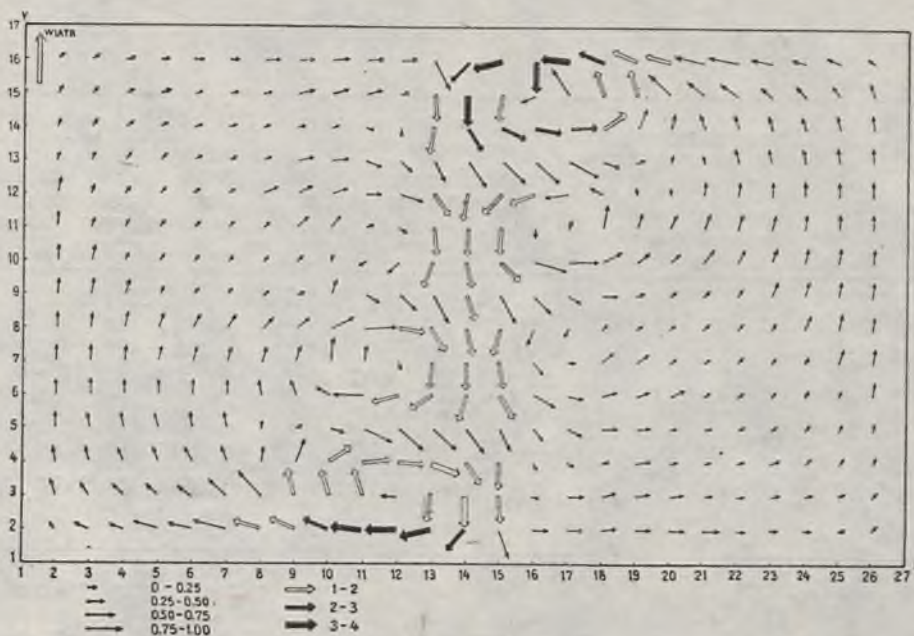
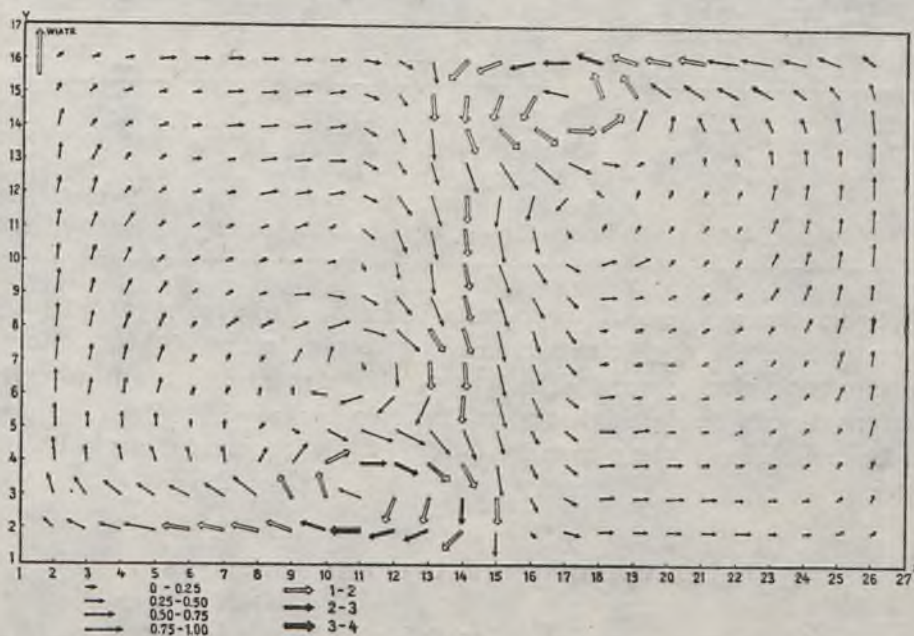
Fig. 7. Field of mass transport vectors ($10^5 \text{ g cm}^{-1} \text{ s}^{-1}$) for case 2Ryc. 7. Pole wydatków masowych ($10^5 \text{ g cm}^{-1} \text{ sek}^{-1}$) dla wariantu 2Fig. 8. Field of mass transport vectors ($10^5 \text{ g cm}^{-1} \text{ s}^{-1}$) for case 3Ryc. 8. Pole wydatków masowych ($10^5 \text{ g cm}^{-1} \text{ sek}^{-1}$) dla wariantu 3

Table 1
Tabela 1

Version Wariant	Time of approaching steady-state (in time steps) Czas ustalania (w krokach τ)	Range of bottom friction factor Zakres zmiany współ- czynnika tarcia przy dnie R s^{-1}	Range of vertical eddy viscosity Zakres zmian współ- czynnika lepkości burzliwej w pionie A $cm^2 s^{-1}$
1	6910	$0.7 \cdot 10^{-4} - 0.3 \cdot 10^{-5}$	const = 420
2	14256	a) $0.2 \cdot 10^{-4} - 0.5 \cdot 10^{-5}$ b) $0.5 \cdot 10^{-4} - 0.3 \cdot 10^{-5}$	a) $108 \div 404 H \leq 78 m$ b) const = 420 $H > 78 m$
3	18550	const = 10^5	const = 150
4	18550	const = 10^5	const = 420
5	18550	const = 10^5	a) $108 \div 404 H \leq 78 m$ b) const = 420 $H > 78 m$

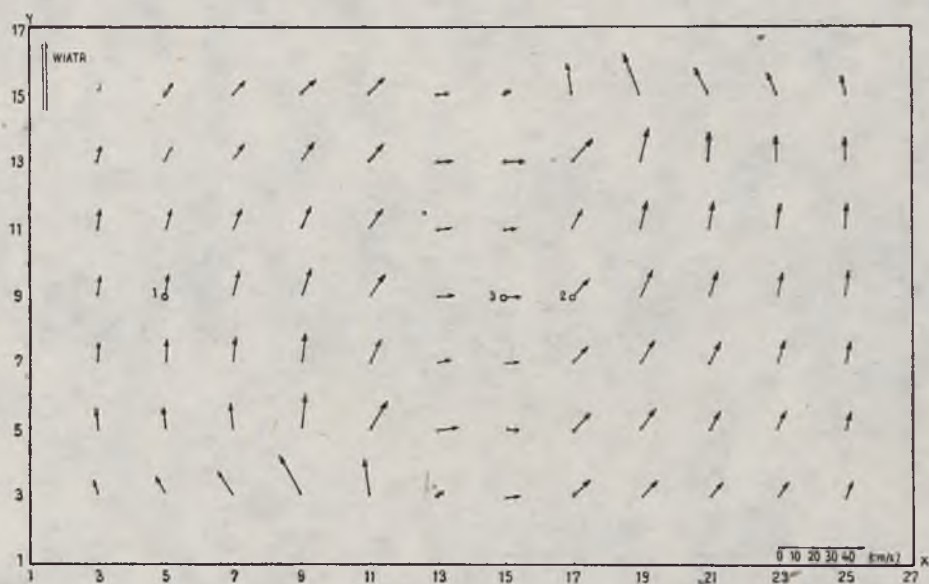
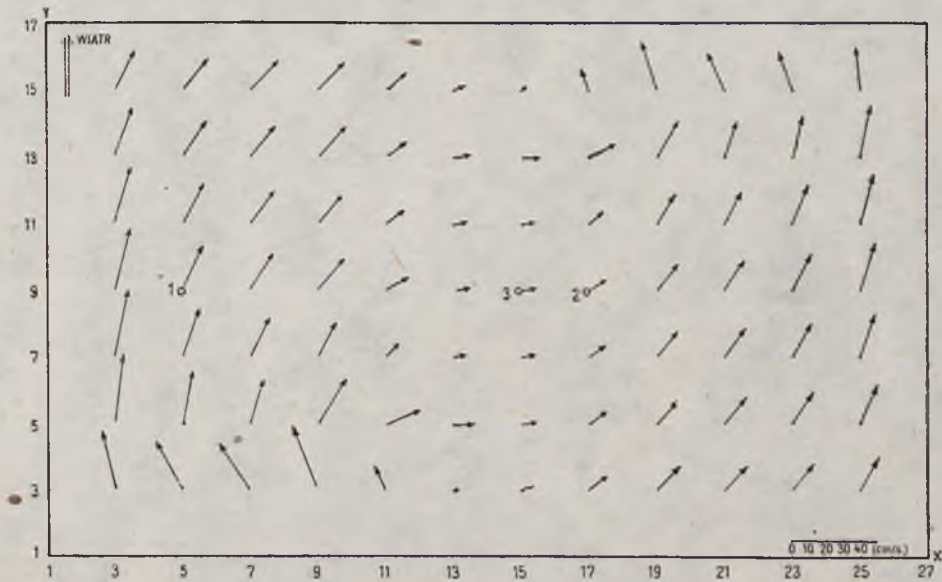
Table 2
Tabela 2

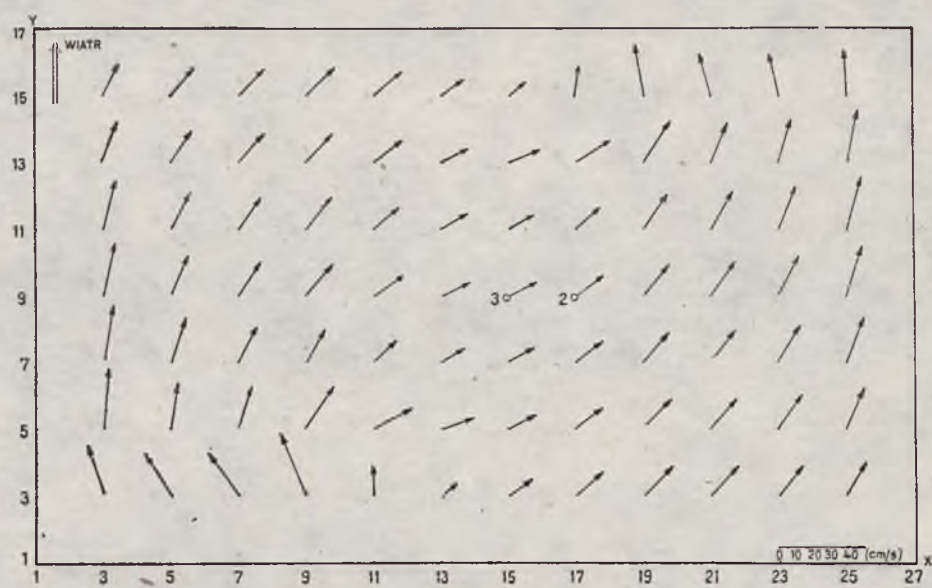
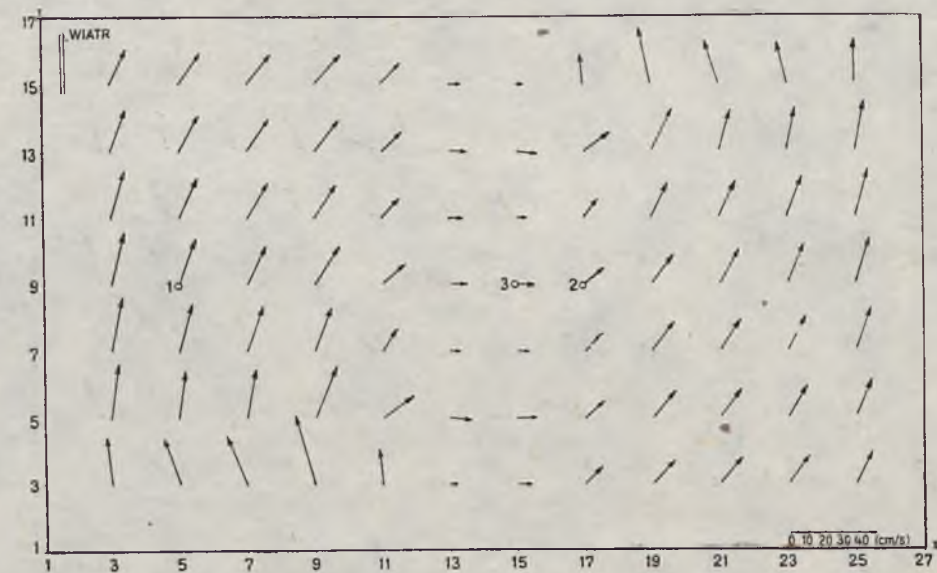
Version Wariant	Time of approaching steady-state (in time steps) Czas ustalania (w krokach τ)	Point 1 Punkt 1 $H = 23,75 m$		Point 2 Punkt 2 $H = 60 m$		Point 3 Punkt 3 $H = 100 m$	
		Coefficient Współczynnik		Coefficient Współczynnik		Współczynnik Coefficient	
		R s^{-1}	A $cm^2 s^{-1}$	R s^{-1}	A $cm^2 s^{-1}$	R s^{-1}	A $cm^2 s^{-1}$
1	6910	$0,58 \cdot 10^{-4}$	420	$0,92 \cdot 10^{-5}$	420	$0,33 \cdot 10^{-5}$	420
2	14256	$0,18 \cdot 10^{-4}$	128	$0,71 \cdot 10^{-5}$	324	$0,33 \cdot 10^{-5}$	420
3	18550	$0,10 \cdot 10^{-4}$	150	$0,10 \cdot 10^{-4}$	150	$0,10 \cdot 10^{-4}$	150
4	18550	$0,10 \cdot 10^{-4}$	420	$0,10 \cdot 10^{-4}$	420	$0,10 \cdot 10^{-4}$	420
5	18550	$0,10 \cdot 10^{-4}$	128	$0,10 \cdot 10^{-4}$	324	$0,10 \cdot 10^{-4}$	420

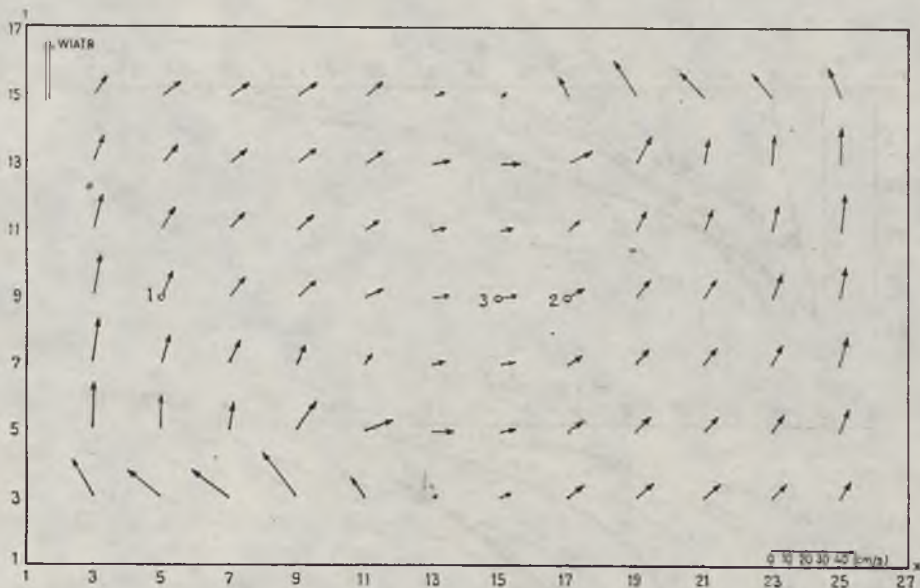
From the analysis of the results it can be inferred that different magnitudes of the coefficients R and A give rise to the differentiation of the current velocities and direction of the current vectors in the five versions. It can be noted that a similar role is played by the magnitude of the coefficients their relationship, and their correlations with the water depth.

6. THE VERTICAL STRUCTURE OF CURRENTS

In order to acquire a deeper insight into the wind-driven circulation the vertical distributions of the current velocity components were computed and the role of the coefficients R and A in the formation of these

Fig. 9. Field of surface currents (cm s^{-1}) for case 1Ryc. 9. Pole prądów powierzchniowych (cm sek^{-1}) dla wariantu 1Fig. 10. Field of surface currents (cm s^{-1}) for case 2Ryc. 10. Pole prądów powierzchniowych (cm sek^{-1}) dla wariantu 2

Fig. 11. Field of surface currents (cm s^{-1}) for case 3Ryc. 11. Pole prądów powierzchniowych (cm sek^{-1}) dla wariantu 3Fig. 12. Field of surface currents (cm s^{-1}) for case 4Ryc. 12. Pole prądów powierzchniowych (cm sek^{-1}) dla wariantu 4

Fig. 13. Field of surface currents (cm s^{-1}) for case 5Ryc. 13. Pole prądów powierzchniowych (cm sek^{-1}) dla wariantu 5

distributions was analysed. Three points of different depths, located as shown in Figs. 9 to 13, were considered.

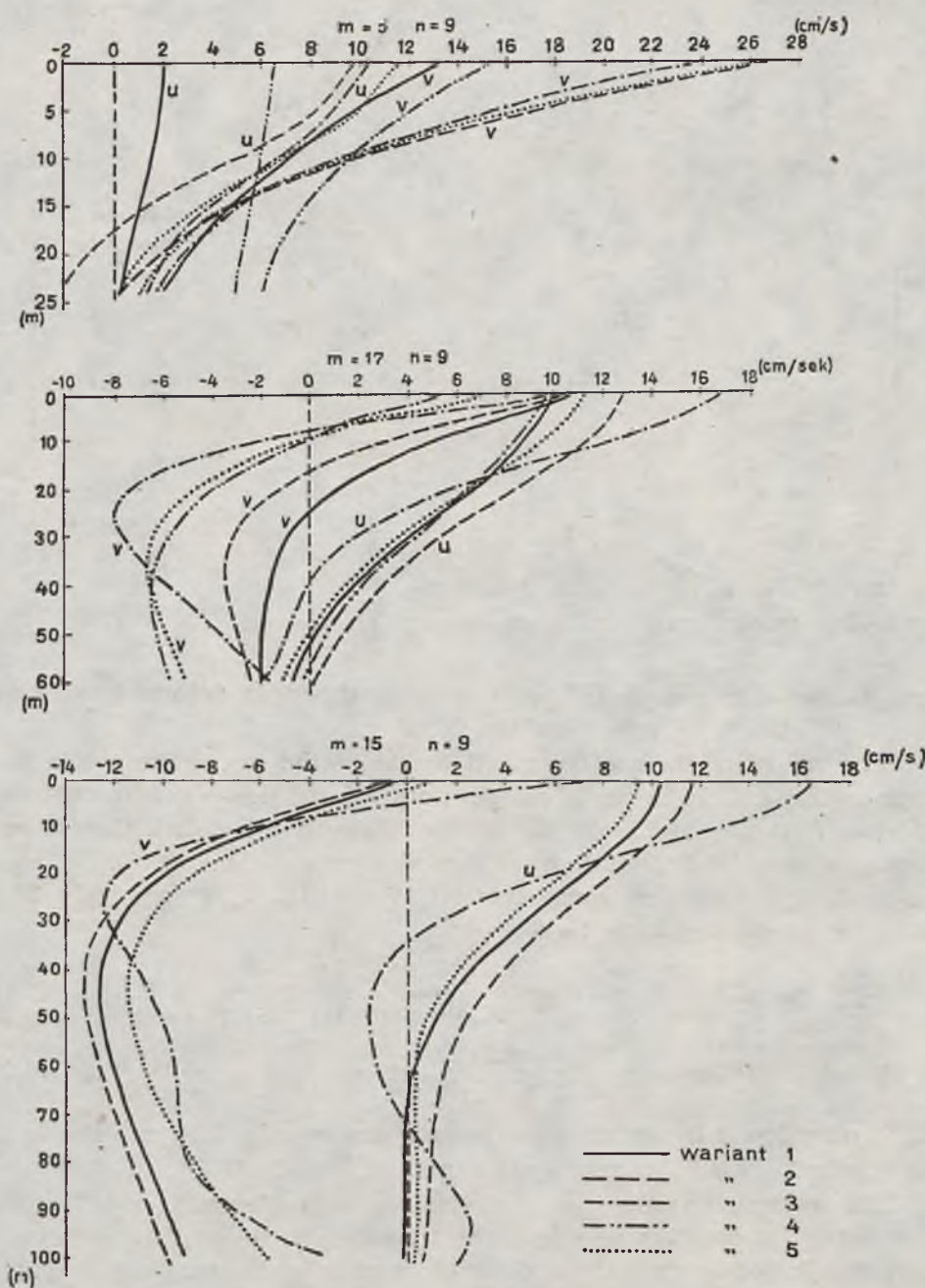
The values of the coefficients R and A at the respective points are given in Table 2. In order to obtain more information about the effects of bottom friction and eddy diffusivity, the vertical distributions were found not only for the total velocity components u and v (2.16), but also for the drift and gradient components U_t , V_t and U_g , V_g , respectively. The latter were computed from the formulae:

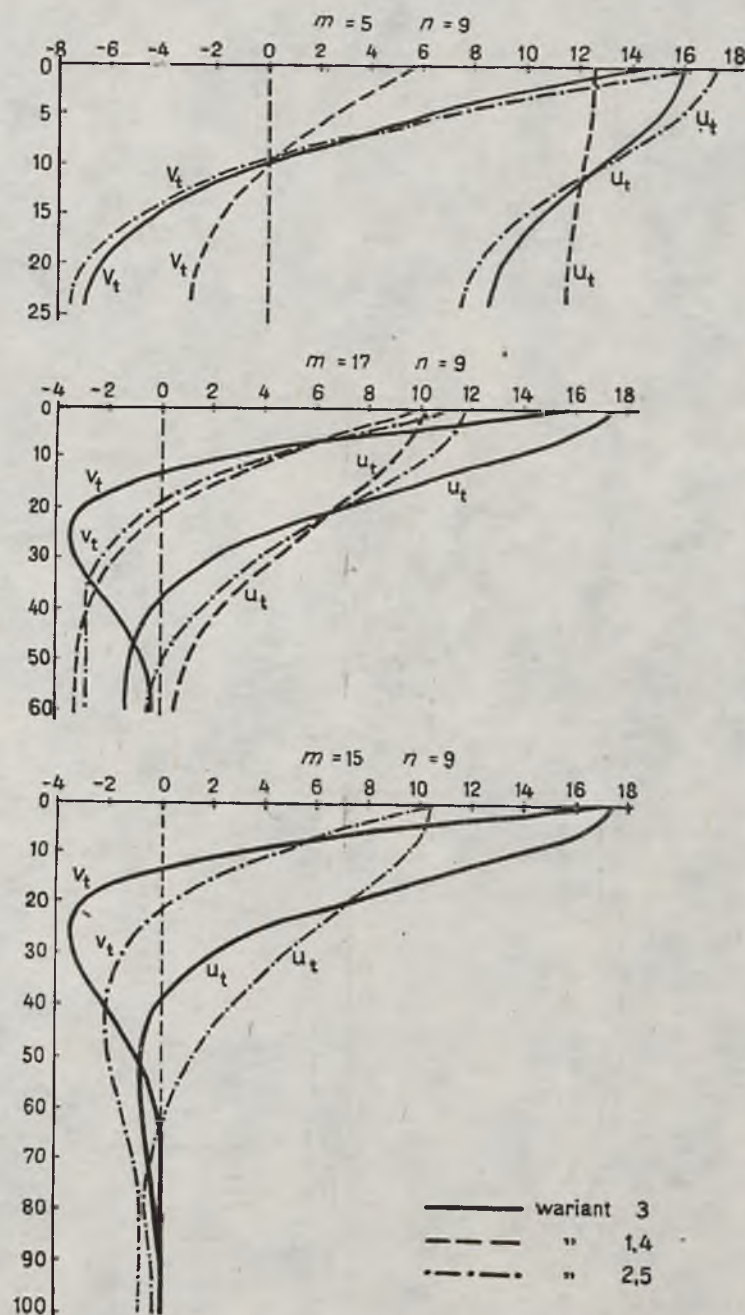
$$D_t = U_t + iV_t = \frac{T}{\rho_0 Ak_1} \frac{\operatorname{ch} k_1 (H+z)}{\operatorname{sh} k_1 (H+\xi)} \quad (6.1)$$

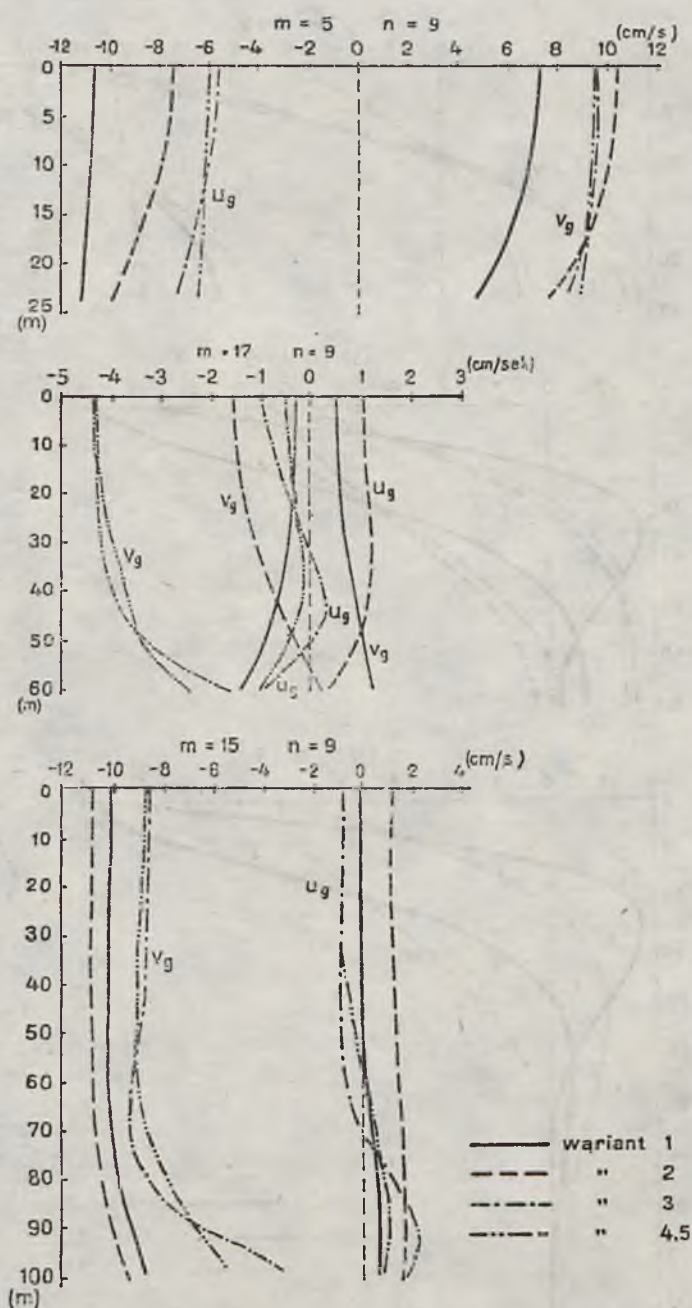
$$D_g = U_g + iV_g = -\frac{RM}{\rho_0 Ak_1} \frac{\operatorname{ch} k_1 (z-\xi)}{\operatorname{sh} k_1 (H+\xi)} + \frac{g}{\Omega} i \left[\frac{\partial \xi}{\partial x} + i \frac{\partial \xi}{\partial y} \right] \quad (6.2)$$

which were found by splitting up the complex velocity 2.16 into the drift and gradient parts. The results are shown in Figs. 14 to 16.

The curves indicate that the vertical eddy viscosity and bottom friction play a considerable role in the formation of the vertical structure currents. The eddy viscosity A determines mainly the drift components, while the friction coefficient R plays a part only in the formation of the gradient components. Similar to the case of the surface currents it can be deduced that not only the size of both coefficients, but also their relationship and correlations with water depths greatly affect the vertical distributions of the current velocity components.

Fig. 14. Vertical distribution of current velocity total components (cm s^{-1})Ryc. 14. Struktura pionowa składowych całkowitych prędkości prądu (cm sek^{-1})

Fig. 15. Vertical distribution of current velocity drift components (cm s^{-1})Ryc. 15. Struktura pionowa składowych dryfowych prędkości prądu (cm sek^{-1})

Fig. 16 Vertical distribution of current velocity gradient components (cm s^{-1})Ryc. 16. Struktura pionowa składowych gradientowych prędkości prądu (cm sek^{-1})

7. CONCLUSIONS

The results of the practical application of the hydrodynamical-numerical scheme H-N in the investigation of the wind-driven circulation permit one to conclude that the differential scheme (2.11—2.13) is stable for all wave-lengths.

The rate of approaching steady-state of the dynamic processes and the structure of the fields of mass transport, sea levels and currents depend much on the bottom friction coefficient. The versions of this coefficient selected and considered in this study show that not only the magnitude of this coefficient, but also its correlations with the sea depth and the vertical eddy viscosity A are of great importance. This is due to the fact that the coefficient A plays a significant role in the formation of current structures, mainly the drift components. The coefficient R affects the fields of mass transport, sea level and gradient components of currents.

The analysis of the fields of surface currents and the vertical structure of currents permits one to conclude that the coefficient A should also be chosen with regard to the configuration of the bottom of a water basin (water depth) and external parameters (the Coriolis force, wind speed etc.).

From the results presented herein the author infers that the most correct results were found in version 2 where both coefficients are interrelated and correlated with water depth, Coriolis force and wind speed.

The Author wishes to express his appreciation to Doc. dr hab. Zygmunt Kowalik from the Institute of Meteorology and Water Management for his remarks and interest during the preparation of this work.

ANDRZEJ JANKOWSKI

Polska Akademia Nauk
Zakład Oceanologii — Sopot

WPŁYW TARCIA PRZY DNIE NA STRUKTURĘ CYRKULACJI WIATROWEJ

Streszczenie

Praca omawia praktyczne zastosowanie metody MTSL (Mass Transport and Sea Level) do badań ustalonej cyrkulacji wiatrowej w jednorodnym akwenie wodnym. Bazą zastosowanej metody jest układ równań nie ustalonych dla wydatków masowych i poziomu morza (2.1—2.3), który całkujemy w czasie ze stałymi siłami wymuszającymi (naprężenie styczne wiatru).

Jako warunek brzegowy na dnie akwenu przyjmujemy liniową zależność naprężenia od składowych wydatku masowego (2.10).

Analiza teoretyczna stosowanej metody [3] wykazała, że kryteria stabilności (2.14—2.15) schematu numerycznego zależą od współczynnika tarcia przy dnie, głębokości akwenu i kroku przestrzennego siatki. Dwie ostatnie wielkości są zazwyczaj uwarunkowane pojemnością pamięci EMC oraz wielkością zbiornika i jedynie współczynnik tarcia przy dnie może być wybrany w dowolny sposób.

Rozważone w pracy warianty wyboru tego parametru (p. 3) wiążą ten współczynnik ze współczynnikiem lepkości burzliwej w pionie, co pozwala ocenić wpływ obu wielkości zarówno na szybkość ustalenia się procesów dynamicznych, jak i na obraz pól wydatków masowych, poziomu morza, prądów powierzchniowych czy pionowych rozkładów składowych prądów.

Do badań wybrano wyidealizowany basen prostokątny z zadanym profilem dna (ryc. 1 i 2). Obliczenia wykonano dla wiatru wiejącego wzduż osi pionowej OY (ryc. 2) ze stałą prędkością 10 m/s.

Rezultaty obliczeń wydatków masowych, poziomu morza oraz prądów wiatrowych dla kilku wariantów wyboru współczynników tarcia przy dnie i lepkości w pionie przedstawiono na ryc. 3—13.

Dla pełnej oceny roli obu parametrów w formowaniu się struktury pionowej składowych prądu oprócz składowych całkowitych (ryc. 14) rozważono również składowe dryfowe (ryc. 15) i gradientowe (ryc. 16).

Przedstawione wyniki pozwalają ocenić nie tylko rolę wielkości obu współczynników, ale także wpływ ich zmienności w obszarze basenu oraz wzajemnego skorelowania.

REFERENCES LITERATURA

1. Druet Cz., Kowalik Z., *Dynamika morza*, Gdańsk 1971.
2. Felzenbaum A.I., *Tieorieticheskie osnovy i metody rasczeta ustaniwiwszichsja morskikh tieczenij*, Moskwa 1960.
3. Jankowski A., *Pewne aspekty zastosowania schematu numerycznego H-N do obliczeń cyrkulacji wiatrowej*, Studia i Materiały Oceanologiczne, nr 16, 1976.
4. Kowalik Z., *Wind-driven circulation in shallow sea with application to Baltic Sea*, Acta Geophys. Pol., 1969.